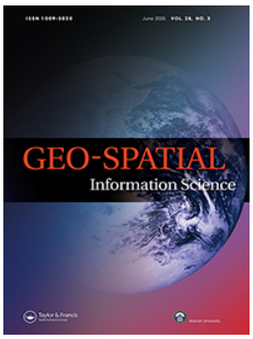

Geo-spatial Information Science

ISSN: 1009-5020 (Print) 1993-5153 (Online) Journal homepage: www.tandfonline.com/journals/tgsi20

A geospatial skeleton framework for unveiling the 3D structure and dynamics of marine heatwaves from earth observation data

Jianing Yu, Hengcai Zhang, Peixiao Wang, Feng Lu & Jicai Ning

To cite this article: Jianing Yu, Hengcai Zhang, Peixiao Wang, Feng Lu & Jicai Ning (29 Aug 2025): A geospatial skeleton framework for unveiling the 3D structure and dynamics of marine heatwaves from earth observation data, Geo-spatial Information Science, DOI: 10.1080/10095020.2025.2547069

To link to this article: https://doi.org/10.1080/10095020.2025.2547069

© 2025 Wuhan University. Published by Informa UK Limited, trading as Taylor & Francis Group.

Published online: 29 Aug 2025.

Submit your article to this journal

View related articles

View Crossmark data

Full Terms & Conditions of access and use can be found at
https://www.tandfonline.com/action/journalInformation?journalCode=tgsi20

GEO-SPATIAL INFORMATION SCIENCE
https://doi.org/10.1080/10095020.2025.2547069

Taylor & Francis
Taylor & Francis Group

OPEN ACCESS Check for updates

A geospatial skeleton framework for unveiling the 3D structure and dynamics of marine heatwaves from earth observation data

Jianing Yu[a,b], Hengcai Zhang[a,b], Peixiao Wang[a,b], Feng Lu[a,b] and Jicai Ning[c]

[a]State Key Laboratory of Resources and Environmental Information System, Institute of Geographic Sciences and Natural Resources Research, Chinese Academy of Sciences, Beijing, China; [b]College of Resources and Environment, University of Chinese Academy of Sciences, Beijing, China; [c]CAS Key Laboratory of Coastal Environmental Processes and Ecological Remediation, Yantai Institute of Coastal Zone Research, Chinese Academy of Sciences, Yantai, China

ABSTRACT
Understanding the multi-dimensional structure and evolution of geospatial phenomena is a fundamental challenge in Earth system science. Marine heatwaves (MHWs), as critical 4D spatio-temporal events in the ocean, exhibit complex vertical heterogeneity and dynamic interactions across latitude, longitude, depth, and time. However, traditional geospatial methods often oversimplify such phenomena into 2D profiles or homogeneous 3D blobs, limiting their ability to capture intrinsic 3D structure and evolutionary patterns. To fill this gap, we propose a novel data-driven framework for constructing 3D skeleton representations of MHWs, enabling fine-grained analysis of their internal structure and spatio-temporal evolution. This framework represents MHW skeletons as graph structure, where nodes denote localized intensity centers and edges quantify morphological correlations of spatial aggregation between subsurface layers. The MHW skeletons are constructed using graph algorithms applied to each snapshot and tracked over time through five evolutionary operators. Applied to the 2014–2016 Northeast Pacific (NEP) and Tropical Pacific in the epipelagic zone (0–200 m), the proposed method reveals distinct vertical structures: ENSO-driven MHW skeletons exhibited greater vertical complexity than coastal MHWs, featuring steep longitudinal slopes (up to 120°). Additionally, two foundational MHW skeleton structures, I-shape and Y-shape, were identified. Notably, dynamic merging and splitting process between subsurface MHWs were captured, highlighting the framework's capability to uncover hidden interactions in ocean systems. Beyond MHWs, this methodology provides a transferable paradigm for analyzing other 3D geospatial phenomena, enhancing our understanding of their structural complexity and dynamic evolution.

ARTICLE HISTORY
Received 9 March 2025
Accepted 7 August 2025

KEYWORDS
Marine heatwaves (MHWs); 3D geospatial structure; 4D spatio-temporal evolution; geospatial skeletons; graph algorithms; Northeast Pacific MHW; ENSO events; ocean temperature anomalies

1. Introduction

The analysis of four-dimensional (4D) geospatial phenomena, characterized by dynamic interactions across latitude, longitude, depth, and time dimensions, is essential for understanding complex Earth system processes (Li et al. 2023; Shu 2016). Among these phenomena, marine heatwaves (MHWs) represent a critical class of oceanic events with cascading ecological (Oliver et al. 2024; Smith et al. 2023), climatic (Capotondi et al. 2024; Oliver et al. 2018), and socio-economic impacts (Holbrook et al. 2020; Smith et al. 2021). Defined as anomalous warm water events persisting for extended periods (Hobday et al. 2016), MHWs are predominantly studied using sea surface temperature (SST) data due to the availability of large-spatial-coverage measurement from satellites. However, subsurface temperature extremes often exhibit greater intensity and persistence than their surface counterparts, affecting deep-sea ecosystems and ocean circulation patterns (Capotondi et al. 2024; He et al. 2024). Expanding MHW research to include subsurface dynamics is crucial for a holistic understanding of these phenomena. Exploring the 3D structure of MHW is a prerequisite for understanding their drivers, impacts, and future projections.

Advances in ocean observation and simulation have led to an explosion of high-dimensional ocean temperature datasets (Cheng et al. 2021; Zhang et al. 2020), enabling deeper insights into MHWs from the surface to ocean interior. Current research (Elzahaby and Schaeffer 2019; Schaeffer, Sen Gupta, and Roughan 2023; Xu et al. 2024) categorizes MHWs into three types: shallow MHWs, which extend from the surface to the upper layer (typically down to 35 m) and fade away below this; extended MHWs, which span the whole water-column and extend deep; and subsurface MHWs, which lack surface expression and exhibit temperature extremes only in the subsurface. These studies focused on vertical temperature anomalies at single locations, but ignored their spatial

CONTACT Hengcai Zhang zhanghc@lreis.ac.cn

© 2025 Wuhan University. Published by Informa UK Limited, trading as Taylor & Francis Group.
This is an Open Access article distributed under the terms of the Creative Commons Attribution License (http://creativecommons.org/licenses/by/4.0/), which permits unrestricted use, distribution, and reproduction in any medium, provided the original work is properly cited. The terms on which this article has been published allow the posting of the Accepted Manuscript in a repository by the author(s) or with their consent.

structure. To address this limitation, a recent study extended the MHW definition from the temporal domain to the spatial-temporal domain, which means that an MHW event should not only have start and end time but also be compact in the space (Sun, Jing, et al. 2023). Building on this, several studies have adopted single-snapshot clustering methods to group spatially proximate anomalies at individual time steps, and subsequently track their evolution over time (Reddy, Perkins-Kirkpatrick, and Sharples 2022; Ren, Wang, and Yao 2025; Sun, Jing, et al. 2023; Sun, Li, et al. 2023). This approach focuses on analyzing discrete temporal snapshots of MHWs, with each time slice capturing a transient state within a continuously evolving system. Although it does not explicitly model dynamic oceanographic processes, it enables the extraction of coherent 3D or 4D MHW structures and supports further analysis of their morphology, displacement, and merging or splitting behavior. Based on the detected spatiotemporally continuous events, a variety of metrics have been developed to describe MHW characteristics, including duration, magnitude, spatial extent, displacement, and deformation (Hobday et al. 2016; Sun, Jing, et al. 2023). In contrast to mechanism-based models, which simulate physical processes based on dynamical equations and require complex initial and boundary conditions, this data-driven method provides a fast, scalable, and interpretable alternative for structural analysis from earth observation data, offering valuable insights into the spatiotemporal extent and evolution of MHW systems.

Despite advances in spatio-temporal clustering methods, most existing approaches treat MHWs as homogeneous blobs in 3D or 4D space, based primarily on spatiotemporal adjacency, without accounting for internal structural variability. However, this simplification fails to reflect the intrinsic heterogeneity of MHWs, both horizontally and vertically. In reality, as illustrated in Figure 1, MHWs can span broad horizontal extents, contain multiple intensity centers, and exhibit complex three-dimensional structures, with shifting thermal cores and varying depths of peak intensity. Consequently, methods based solely on adjacency may misclassify fragmented or structurally complex MHWs as a single coherent event, masking important physical distinctions. This structural complexity highlights the need for analytical frameworks that move beyond simple adjacency-based metrics (e.g. duration, spatial extent, displacement) and can effectively represent the fine-scale three-dimensional structure of MHWs.

Recent advancements in geospatial information science emphasize the need for multi-dimensional analytics to resolve such fine-scale spatial variability (Ding et al. 2024; Yu, Yang, and Jin 2018; Zhang et al. 2011). Among various approaches, graph-based skeletons have notable advantages in representing and analyzing spatial structures in three dimensions (Borgefors, Nyström, and Di Baja 1999; Peizhi and Lai 2002; Zou et al. 2023). Inspired by these advances, we propose a novel data-driven framework for constructing 3D skeleton representations of MHWs, enabling fine-grained analysis of their internal structure and spatio-temporal evolution. By abstracting MHWs into graph structures composed of nodes and edges, our framework captures spatial organization, aggregation characteristics, and the evolving dynamics within clustered MHW regions. The main contributions of this paper are as follows:

- **Concept of 3D Skeleton for MHWs**: We propose the concept of MHW skeleton to represent their internal structure for the first time. The skeleton

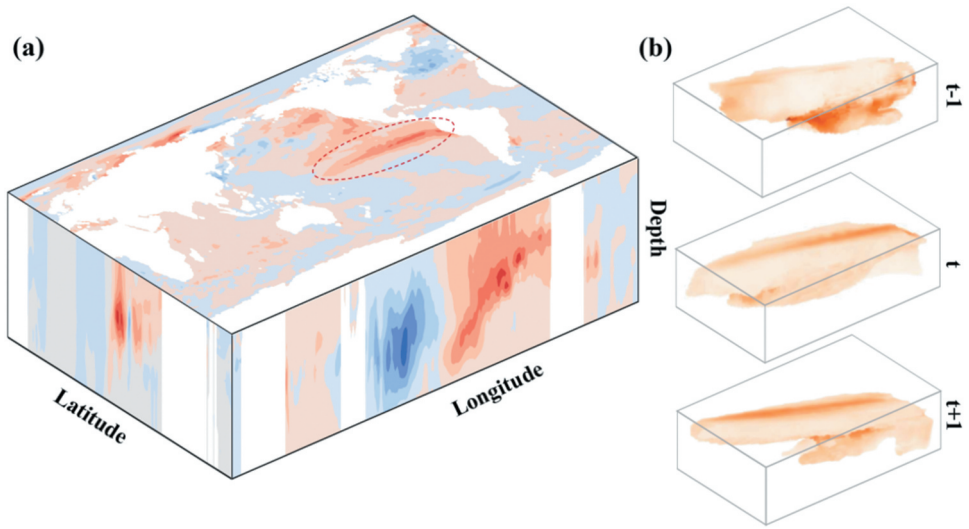

Figure 1. Schematic diagram for the challenge of identifying the true 3D structure of MHWs. (a) Horizontal and vertical heterogeneity of 3D ocean temperature; (b) spatial compact MHWs sliced at three different times.

is composed of nodes representing the intensity centers and edges representing the morphological correlations of spatial aggregation, effectively quantifying the fine-grained 3D structure of MHWs.

- **Framework for modeling MHW Skeletons**: We present a data-driven computational framework for constructing, characterizing and tracking MHW skeletons. Skeletons are built using graph algorithms applied to each snapshot and are tracked across time based on five evolutionary types: continuation, merging, splitting, generation, and dissipation.
- **Application to the historical MHW events**: We apply this method to the 2014–2016 Northeast Pacific (NEP) and Tropical Pacific in the epipelagic zone (0-200 m). By analyzing their time-evolving skeletons, we reveal unique vertical structures and evolutionary trajectories over their lifecycles, demonstrating the utility of the skeleton approach for improving our understanding of large-scale ocean heatwave events.

The rest of this paper is organized as follows: Section 2 outlines the dataset and method, including the definition and properties of MHW skeletons, and the construction process involving node extraction and edge construction. This section also introduces evolution operators for analyzing MHW skeletons. Section 3 presents the results, covering the accuracy of MHW identification and detailed analyses of skeleton characteristics. Section 4 discusses the findings and their implications, while Section 5 concludes with a summary of contributions and future research directions.

2. Materials and methods

This section presents a systematic framework for constructing and analyzing 3D MHW skeletons. We begin by introducing the ocean temperature dataset and study area (Section 2.1). Next, we give the definition and properties of MHW skeletons as graph structures that preserve reconstructability and reliability (Section 2.2). The skeleton construction workflow is then detailed in Section 2.3. Finally, we establish evolution operators for tracking temporal transitions (Section 2.4).

2.1. Data and study area

The study area spans 120°E–80°W and 30°S–60°N, which covers the 2014–2016 El Niño-Southern Oscillation (ENSO) in the tropical Pacific and the concurrent Northeast Pacific MHW (NEP MHW), as shown in Figure 2(a). We focus on the period from 2014 to 2016, which captures the full lifecycle of these well-documented events, including their development, peak, and dissipation phases (Tseng, Ding, and Huang 2017). This timeframe provides an ideal testbed for evaluating the proposed skeleton framework due to the events' extraordinary magnitude and widespread environmental consequences. Additionally, selecting this period facilitates direct comparison with previous studies (Sun, Jing, et al. 2023) and highlights the methodological advancements of our approach. Monthly IAP sea temperature data (IAPv4, http://www.ocean.iap.ac.cn/ftp/cheng/IAPv4_IAP_Temperature_gridded_1month_netcdf/) were used to identify MHW events. IAPv4 provides monthly 1°*1° grid snapshots from the surface to 6000 m (119 layers) covering the period from 1940 to present. The sea temperature data were resampled into 1°*1°*10 m grids over the upper 200 m covering the epipelagic zone, which is ecologically critical and home to a vast diversity of marine organisms. (Figure 2(b)). While daily sea temperature data is commonly used to capture short-term extremes and event duration, monthly data is more appropriate for this study, which focus on long-lasting, large-scale MHWs and their

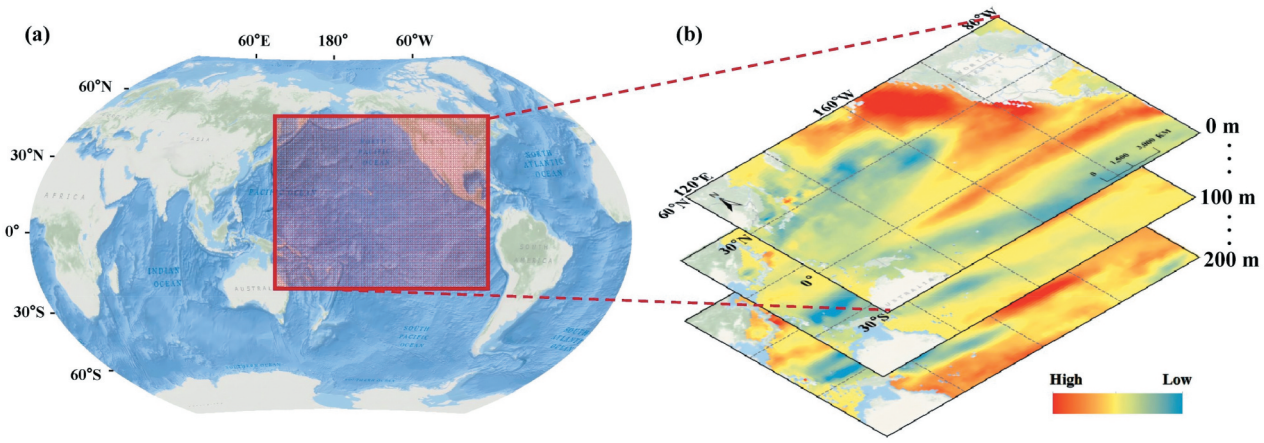

Figure 2. Data and study area. (a) Study area on a global scale. (b) Monthly sea temperature anomalies averaged over 2014–2016 relative to the 1990–2020 climatology within the research scope.

structural evolution. The use of monthly data reduces high-frequency variability, enhances spatial and vertical coherence, and improves computational feasibility when handling three-dimensional datasets across extended time periods.

2.2. Definition and properties of 3D MHW skeletons

2.2.1. Definition

The skeletons of MHW are derived from 3D MHW candidate, which are defined as discrete, prolonged, and anomalously warm water events with compact spatial structures, following the definition proposed by (Sun, Jing, et al. 2023). Figure 3(a) illustrates a 3D MHW candidate identified through spatial connectivity, characterized by multiple intensity centers at each depth layer.

MHW skeletons are conceptualized as undirected graphs, which model a set of objects (nodes or vertices) and their interactions (edges), expressed as $G = (V, E)$. In this framework, each node corresponds to a local maximum of MHW intensity at a specific depth, and each edge represents the morphological correlations between a pair of intensity centers at the aggregation scale across adjacent depth layers. As shown in Figure 3(b), intensity peaks $V_d = \{v_1, v_2, \ldots, v_n\}$ are defined as the grid points whose MHW intensity exceeds that of all surrounding values within a moving window at depth d. When intensity peaks are separated by distances larger than the window size, multiple nodes are identified within the same layer. These local maxima capture the thermodynamically meaningful cores of MHWs and provide a more accurate representation of the physical centers of heat anomalies than geometric centroids, which only reflect spatial averages and may lie in areas of moderate intensity. Serving as physically meaningful seeds, these intensity peaks guide a segmentation process that partitions the broader MHW into subregions, referred to as MHW cells, centered around each thermal anomaly core. A skeleton node is described by its spatial coordinates (latitude, longitude, depth) and attributes, including the intensity and size of its corresponding MHW cell. MHW cells at different depths, when connected based on physically informed criteria (Section 2.3.3), form a fine-grained 3D MHW. Figure 3(c) demonstrates that the 3D MHW candidate is subdivided into two fine-grained 3D MHWs, represented by different colors.

2.2.2. Properties

The proposed MHW skeletons serve as an effective abstraction of 3D MHW structures. To ensure their representational validity, we emphasize two essential properties: reconstructability, which refers to the ability to recreate the full 3D geometry of an MHW from its nodes and vertical edges; and representativeness ensures that all thermo-dynamically significant regions are represented by at least one node. These properties confirm that the skeleton preserves key features of the original intensity field and captures all critical regions within the MHW structure. Importantly, these properties are not automatically satisfied and must be explicitly considered to avoid structural omissions or distortions. For instance, replacing local-maximum nodes with geometric centroids, which average spatial coordinates, may misrepresent the heat distribution, thereby compromising reconstructability.

2.3. Construction of 3D MHW skeletons

Figure 4 presents the overall workflow of the proposed geospatial skeleton framework for identifying, constructing, and tracking the 3D structure and evolution of MHWs. The framework consists of three main steps. First, 3D candidate MHW snapshots are extracted from sea temperature anomalies using widely accepted thresholding and adjacency criteria. Then, based on the extracted clustered MHWs, skeletons are built by identifying intensity-based nodes and establishing vertical edges between them to represent internal structure. Finally, the temporal evolution of

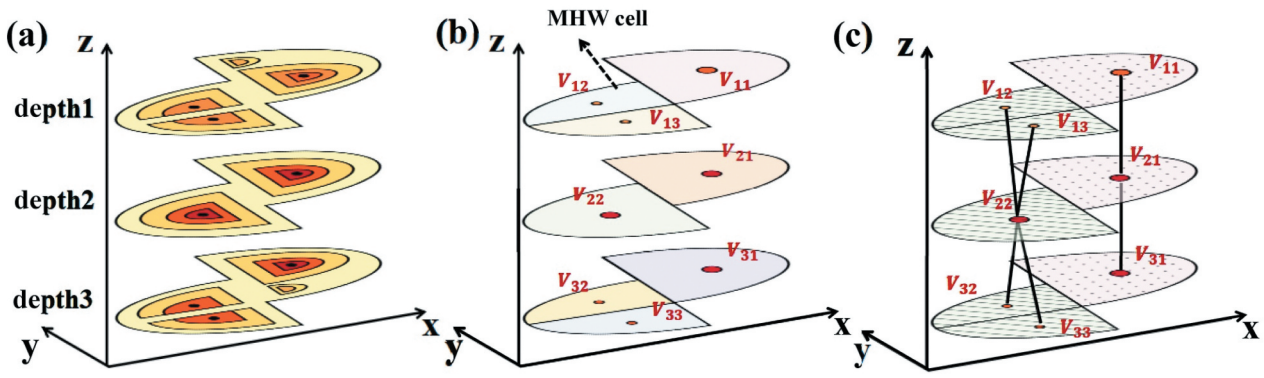

Figure 3. Schematic diagram for MHW skeletons. (a) A 3D candidate MHW snapshot based on continuity. (b) Intensity centers and segmented MHW cells. (c) Skeletons of fine grained 3D MHW.

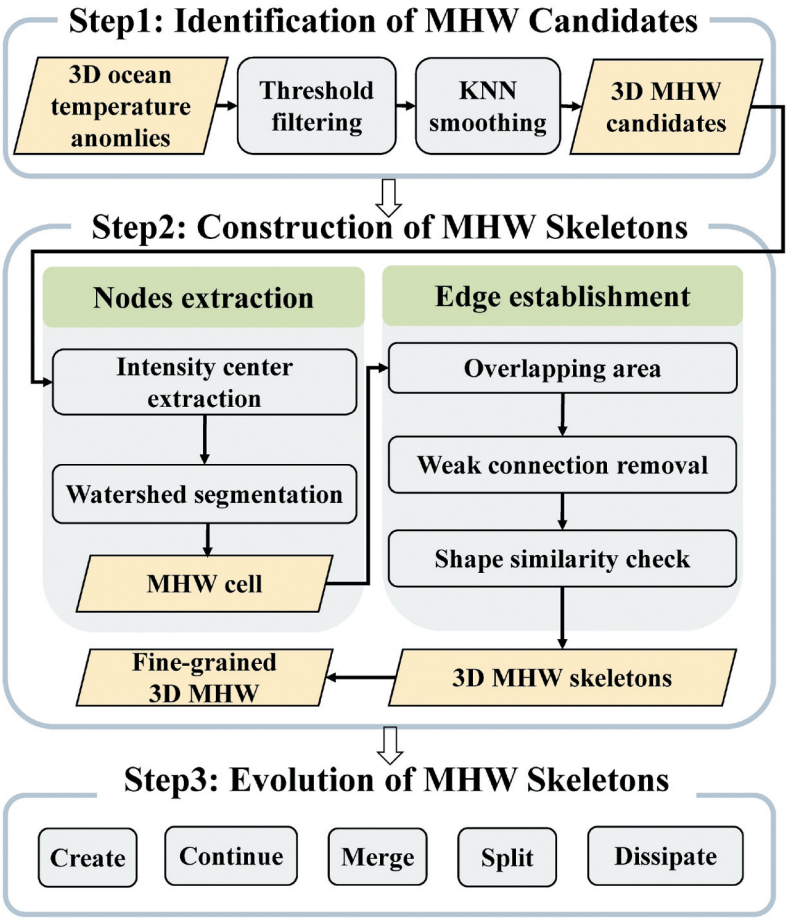

Figure 4. Flowchart for the MHW skeleton framework.

these skeletons is characterized using five defined operators.

2.3.1. Identification of MHW candidates

First, we calculated time series of marine temperature anomalies relative to the 1990–2020 baseline climatology at each grid. The 30-year baseline (1990–2020) follows the climatological reference standard recommended by the World Meteorological Organization (WMO), which encourages updating the baseline every decade to better reflect ongoing climate change. This selection is also consistent with commonly used MHW detection methods (Hobday et al. 2016). To reduce the influence of interannual variability and isolate anomalous warming, a monthly climatology approach was applied. For example, January anomalies were calculated against the average January temperatures from 1990 to 2020. This method effectively removes the seasonal cycle and improves the robustness of MHW detection. Grids with anomalies above a seasonally varying 90th-percentile threshold are identified as MHW candidate grids in the temporal domain.

To ensure spatial coherence, k-nearest-neighbor (KNN) method is used to account for the spatial dependence of temperature (Sun, Jing, et al. 2023). A grid cell is categorized as MHW only if more than half of its K-nearest grid cells are identified as MHW on the raw MHW snapshots. Spatially connected grids were then grouped to form three-dimensional MHW candidates. This procedure can be formally expressed as:

$$KNN(Thre_{90}(SSTA)) = \{C_1, C_2, \ldots, C_k\}, \quad (1)$$

where each C_k denotes a spatially connected MHW candidate cell satisfying the KNN-based continuity condition. As the KNN smoothing may misrepresent small-volume MHW candidates, we discard MHW candidates occupying less than $K3$ grid cells to reduce the influence of small, short-lived, or potentially noisy features. The performance of KNN is sensitive to the choice of the K-parameter. Based on sensitivity experiments (see Section 3.4.1), we selected $K = 5 \times 5 \times 5$ for the 1°×1°×10 m dataset in this study, which effectively captured spatially coherent MHW structures without distorting the representation of major events.

2.3.2. Nodes extraction

The skeleton joints, representing the local maximum intensity points of each layer, were extracted based on the moving window method. For each grid $P_{id}(lat, lon)$ at depth d in the i-th MHW candidate C_i, a moving window was centered at P_{id}. If the intensity of grid P_{id}

(lat, lon) exceeded all other values within the moving window W, $P_{id}(lat, lon)$ was considered as an intensity center v_{id}. The watershed algorithm (Meyer 1992) was then used to segment the MHW cells associated with each intensity center.

The watershed algorithm is a widely adopted image segmentation technique used in geospatial analysis. In this framework, it treats the intensity field as a topographic surface, where higher intensity values represent peaks and lower values represent valleys. Figure 5(a) shows a horizontal slice of a 3D MHW candidate. Local maxima are selected as seed points (Figure 5(b)), from which virtual water is simulated to flow outward along intensity gradients (Figure 5(c)). When water from different peaks meets, watershed boundaries (labeled as W) are formed to separate thermally distinct regions (Figure 5(d)). The inputs of the watershed segmentation algorithm were each horizontal slice of i-th MHW candidates at depth d, denoted as C_{id} and intensity center set $V_{id} = \{v_1, v_2, \ldots, v_n\}$ as seeds. The outputs were MHW cells, with a pixel value of −1 at watershed W, and values of each MHW cell were assigned corresponding labels of seed set V_{id} (Equation (2)). The saliency was defined to be the areal extent of the basin referring to Lakshmanan, Hondl, and Rabin (2009).

For each i in range (k), for each d in range (*depth*),

$$Watershed(C_{id}, V_{id}) = \begin{cases} -1, \text{if}(x, y) \in W \\ label(V_{id}), \text{else} \end{cases}, \quad (2)$$

where k is the total number of MHW candidates, and *depth* is the number of vertical layers of MHWs.

2.3.3. Edge establishment

Then, the edge connection criteria between a pair of MHW cells were based on the assumption that a 3D MHW snapshot should change gradually rather than abruptly with depth. A small depth step was expected to result in minimal deformation and displacement. Consequently, MHW cells on adjacent layers were connected if they significantly overlapped and exhibited similar shapes. It is important to emphasize that these edges are not intended to represent physical coupling or oceanic mixing processes. Instead, they provide a data-driven abstraction of the internal structural organization within the previously identified MHW volume. The establishment of edges involves three key steps.

First, for any pair of MHW cells on adjacent layers, the overlapping area ratio (OAR) is calculated as the ratio of the overlapping area to the area of the smaller cell. If the OAR exceeds 50%, a preliminary edge is established between the two cells. However, these preliminary connections may contain weak edges, which can erroneously link MHW cells into a single oversize MHW (see Figure 6(a), e.g. edge ⑤). To address this issue, we introduce the concept of communities within the MHW skeleton graph.

A community is defined as a group of MHW cells (nodes) that are tightly connected through strong spatial association across adjacent layers. In the graph-theoretic sense, it corresponds to a subgraph where nodes are more densely connected to each other than to nodes in other parts of the graph. In this context, weak connections refer to edges between nodes that belong to different communities. These edges typically indicate poor spatial correlation and should be pruned to avoid erroneous merging of distinct MHW components.

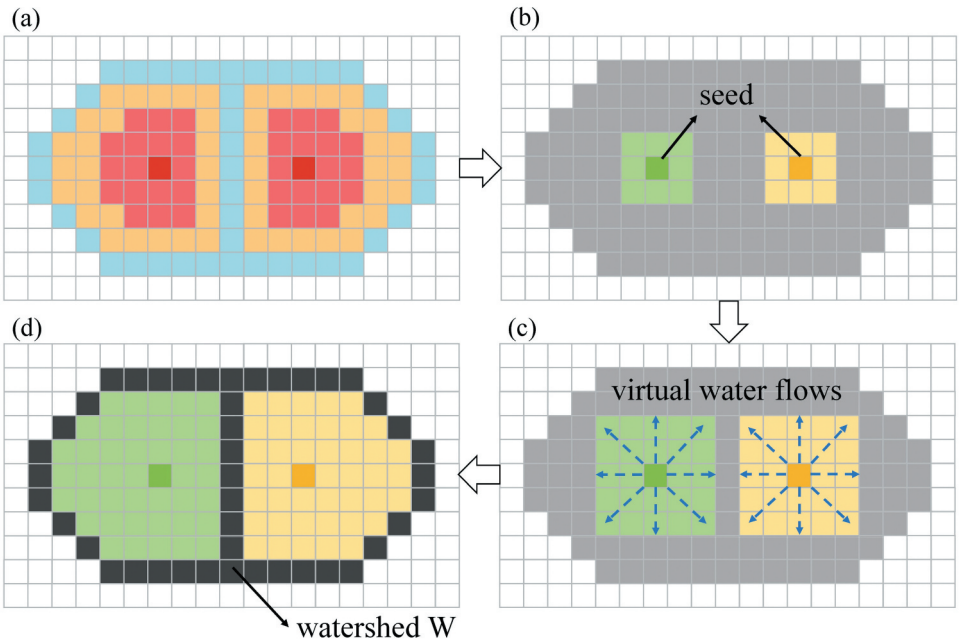

Figure 5. Schematic diagram for watershed algorithm. (a) Slice of the i-th MHW candidate at depth d; (b)–(c) the process of virtual water flowing outward from seeds; (d) watershed segmentation results.

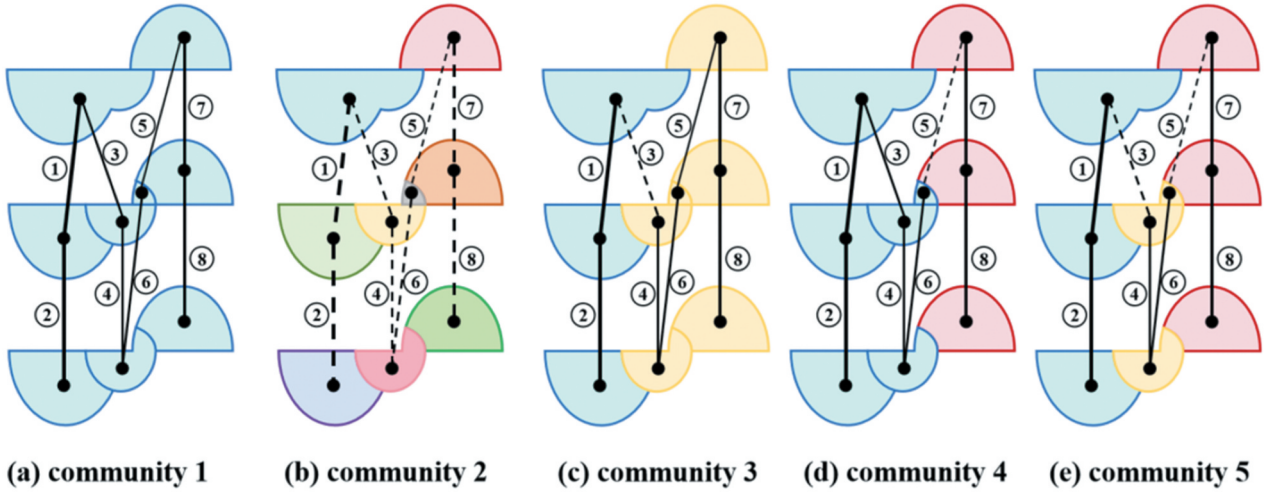

Figure 6. Five different community combinations. The thickness of the edge indicates the high or low OAR value.

To detect and remove such weak connections, we apply a modified Louvain algorithm (Que et al. 2015) that maximizes modularity under a layered-graph constraint. In our formulation, each node represents an MHW cell, and edges are only allowed between nodes in adjacent depth layers. We define a modified Modularity Q, which includes two terms. The first item represents the sum of the weights of intra-community edges (favoring strong internal connectivity). The second item represents a penalty for how far each community deviates from being fully connected (discouraging sparse groupings).

$$Q = \sum_{d=0}^{depth-1} \left(\sum_{i,j} W_{A_{d,i}}^{d+1,j} \delta(V_i, V_j) - \sum_{i,j} (1 - W_{B_{d,i}}^{d+1,j}) \delta(V_i, V_j)\right),$$

$$W_{A_{d,i}}^{d+1,j} = Normalize(OA_{d,i}^{d+1,j}) + Normalize(\max - EucDis_{d,i}^{d+1,j}) \quad if\ OAR_{\mathrm{d,i}}^{d+1,j} > 0.5,$$
$$W_{B_{d,i}}^{d+1,j} = 1\ if\ OAR_{\mathrm{d,i}}^{d+1,j} > 0.5, \tag{3}$$

where $\delta(V_i, V_j)$ determine whether node i and node j belong to the same community. If so, the value is 1; otherwise, it is 0. $W_{A_{d,i}}^{d+1,j}$ and $W_{B_{d,i}}^{d+1,j}$ represents the weight between nodes i and j, W_A depends on the overlap area of 2D MWH units and the Euclidean distance between nodes, W_B are all 1 when the OAR is greater than the threshold.

As shown in Figure 6, five possible community combinations are illustrated to demonstrate the impact of different grouping strategies. The calculation process of Q is shown in Table 1. When all MHW cells are merged into one community (Figure 6(a)), the first term in Q is maximized, but the second term also incurs a high penalty due to sparse connectivity. When each cell is treated as a separate community (Figure 6(b)), both terms equal zero. The optimal configuration is illustrated in Figure 6(e), where three compact communities are identified. Although its first term is not the highest, its second term is minimized (zero), resulting in the maximum overall Q value.

Finally, a shape similarity check is conducted to refine the skeletons further. After eliminating weak connections, two MHWs are merged if the similarity of the combined 2D MHW cells across adjacent depths increases post-merging. Shape similarity is quantified using Hu Moments (Žunić, Hirota, and Rosin 2010), implemented via the matchShapes function from the OpenCV Python library.

2.4. 4D evolution of MHW skeletons

Five evolution operators, including continuation, merging, splitting, creation and dissipation (Table 2), were used to track the MHW events temporal transition. The evolution operator was determined based on the overlapping volume ratio (OVR) between 3D fine-grained MHWs identified in the previous step at two consecutive time steps. The OVR between consecutive time steps is calculated as the ratio of overlapping MHW volume to the smaller of the two volumes. For each $MHW_{t,i}$, its successor $MHW_{t+1,j}$ is identified as the one whose

Table 1. The calculation process for Modularity Q.

	First item	Second item	Q
community 1	9.67	20−8 = 12	−2.33
community 2	0.00	0−0=0	0.00
community 3	9.67−0.33 = 9.34	(2−2)+(9−5) = 4	5.34
community 4	9.67−0.00 = 9.67	(9−5)+(2−2) = 4	5.67
community 5 (best)	9.67−0.33−0.00 = 9.34	(2−2)+(2−2)+(2−2) = 0	9.34

Table 2. Temporal transition for MHW skeletons.

Temporal transition	Diagram	Description	Formulae
Continuation	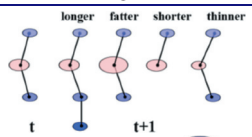	The MHW_i at time t and the MHW_j at time t+1 only overlap each other with OVR exceeding the threshold.	$\exists i \in M_t, \exists j \in M_{t+1}$, $OVR_{t,i}^{t+1,j} > \alpha$.
Merging	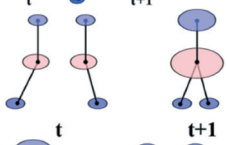	The MHW_j at time t+1 overlaps with multiple MHWs at time t with OVR exceeding the threshold.	$\exists i_1, i_2 \in M_t, i_1 \neq i_2$, $OVR_{t,i_1}^{t+1,j} > \alpha$, $OVR_{t,i_2}^{t+1,j} > \alpha$.
Splitting	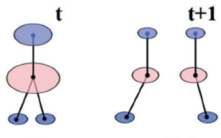	The MHW_i at time t overlaps with multiple MHWs at time t+1 with OVR exceeding the threshold.	$\exists j_1, j_2 \in M_{t+1}, j_1 \neq j_2$, $OVR_{t,i}^{t+1,j_1} > \alpha$, $OVR_{t,i}^{t+1,j_2} > \alpha$.
Creation	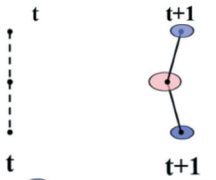	The MHW_j at time t+1 does not overlap with any MHW at time t.	$i \in M_t, OVR_{t,i}^{t+1,j} < \alpha$.
Dissipation	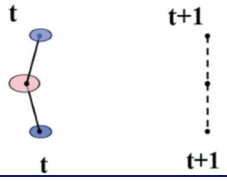	The MHW_i at time t does not overlap with any MHW at time t+1.	$j \in M_{t+1}, OVR_{t,i}^{t+1,j} < \alpha$.

$OVR_{t,i}^{t+1,j}$ exceeds a prescribed threshold α. Referring to previous research, the alpha value in this article is 0.5 (Sun, Jing, et al. 2023; Sun, Li, et al. 2023).

3. Results

3.1. Accuracy of MHW identification

To assess the effectiveness of the proposed method, we conducted comparative experiments against the Tracking Strategy outlined by Sun, Jing, et al. (2023); Sun, Li, et al. (2023). This benchmark approach tracks MHW events based on spatial overlap and centroid distance, assigning merged regions according to proximity and overlap with prior events. Our comparison reveals that, in general, the structural patterns identified by our skeleton-based method are broadly consistent with those reported in Sun, Jing, et al. (2023); Sun, Li, et al. (2023), particularly in terms of spatio-temporal extent and overall event boundaries. However, our method offers enhanced resolution in capturing finer structural details, especially in complex events characterized by multiple intensity peaks. Specifically, our method accounts for the continuity of MHWs across both horizontal and vertical dimensions, producing MHW structures that are spatially continuous in 3D (Figure 7(f-h)). In contrast, the Tracking Strategy enforces continuity in only one dimension, often resulting in fragmented MHWs along the horizontal plane (Figure 7(c-e)). Furthermore, our method integrates the distribution of temperature anomalies, under the assumption that each MHW cell at a given depth contains a single intensity center. This ensures a closer alignment with the actual contour distribution of MHWs. For instance, in Figure 7(j) , the intensity of the equatorial Pacific MHW at 100 m depth decreases radially from the center and features two intensity centers. The surrounding MHW intensity varies according to the central regions, making the Tracking Strategy's identification of separate MHWs for strong central regions and weaker peripheries inaccurate (Figure 7(d)). Our method addresses this limitation by accurately delineating regions belonging to each intensity center, as illustrated in Figure 7(g).

3.2. Structure of MHW skeletons

The fine-grained extraction results of three representative MHWs at critical time points are shown in Figure 8, and their skeletons for April 2015 are shown in Figure 9. The "ARC"-like pattern (Di Lorenzo and Mantua 2016) in Figure 8(b) is constituted with three main MHWs: the MHW located at the Gulf of Alaska (hereinafter referred to as GOA MHW), the MHW along part of the Pacific North American coastline from California and Mexico (hereinafter referred to as Cali-Mex MHW), and the MHW in the tropical Pacific (hereinafter referred to as ENSO MHW). ARC refers to the arcuate (curved) spatial pattern of the MHW, resembling the structure commonly associated with the Pacific Decadal Oscillation.

The MHW skeletons in Figure 9 reveal distinct vertical structures among the three MHWs in both

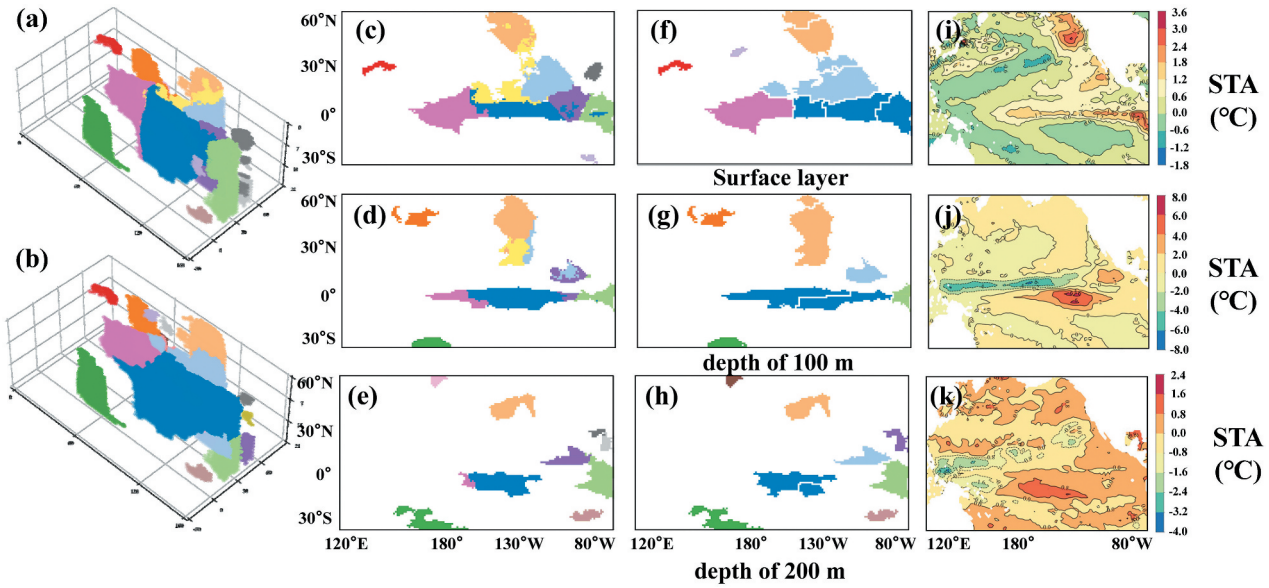

Figure 7. Comparison between 3D MHWs at May 2015 extracted based on (a) tracking strategy and (b) our method. (c) – (e) and (f) – (h) are slices of (a) and (b) at surface, 100m, and 200m depths respectively. (i) – (k) are contours of temperature anomaly at surface, 100m, and 200m depths. White lines in figure 7(f-h) denote watershed boundaries that separate MHW cells, highlighting internal substructures centered on distinct intensity maxima. Cells connected by skeleton lines and sharing the same color belong to the same 3D MHW.

intensity and distribution. The GOA MHW exhibited peak intensity within the 0 m–70 m depth range. In contrast, the Cali-Mex MHW was characterized by high intensity not only at the surface but also extending to depths of 70 m–120 m. Meanwhile, the ENSO MHW exhibited elevated intensity predominantly between 60 m–130 m. The skeleton of GOA MHW displayed the smallest degree of curvature, while the other two exhibited greater curvature, indicating stronger vertical heterogeneity of intensity distribution.

From the latitude-depth profile (Figure 9(g-i)), the latitude of these three MHWs' skeletons changed little with depth, located at 45°N, 15°N, and 0°, respectively. In contrast, the longitude-depth profile (Figure 9(d–f)) varied among MHWs. The skeleton of the Cali-Mex MHW exhibited a longitudinal shift with depth, appearing farther east at 200 m compared to the sea surface. The skeleton of the ENSO MHW exhibited a Y-shape in the longitude-depth profile and an inverted Y-shape in the latitude-depth profile. This finding indicates that two intensity centers at longitude 180° and 120°W between 0–120 m transformed into one center at 120 m–200 m, while the intensity center at latitude 0° between 0–50 m split into two intensity centers at 5°S and 5°N between 50 m–180 m. From the surface to 200 m, the nodes of the ENSO MHW skeleton shifted from east to west. The depth-varying intensity profiles (Figure 9(j–l)) are consistent with the vertical structure classifications proposed by Zhang et al. (2023). Specifically, the GOA MHW exhibits characteristics of the Deep MHW type, marked by surface warming that gradually diminishes with depth yet penetrates several hundred meters, typically associated with subduction and heat transport by western boundary currents or eddies. In contrast, the Cali-Mex and ENSO MHWs correspond to the Subsurface-intensified type, with peak warming at approximately 70 m and 120 m, respectively, often resulting from subsurface heat accumulation driven by advection and modulated by large-scale climate variability.

3.3. Evolution of MHW skeletons

As shown in Figure 10(a), from January 2014 to January 2016, the skeletons of GOA, Cali-Mex and ENSO MHW evolved independently. From February to December 2016, the evolution process became more complex. During 2016, GOA and Cali-Mex MHW merged first, and then ENSO MHW split into two parts, one of which merged with the GOA and Cali-Mex MHW. The animations of the skeletons of these MHWs can be further viewed through https://doi.org/10.6084/m9.figshare.29322473.

As illustrated in Figure 10(b), the GOA MHW evolved from three MHWs, similar to the findings of Sun, Jing, et al. (2023). When the GOA MHW entered a period of decline, the intensity and area of MHW cells at sea surface decreased before those of the interior of the ocean, corroborating the long-term memory of ocean proposed by Scannell et al. (2020). Additionally, Figure 10(c) indicated that the Cali-Mex MHW evolved from the surface to the interior of the ocean, reaching its maximum

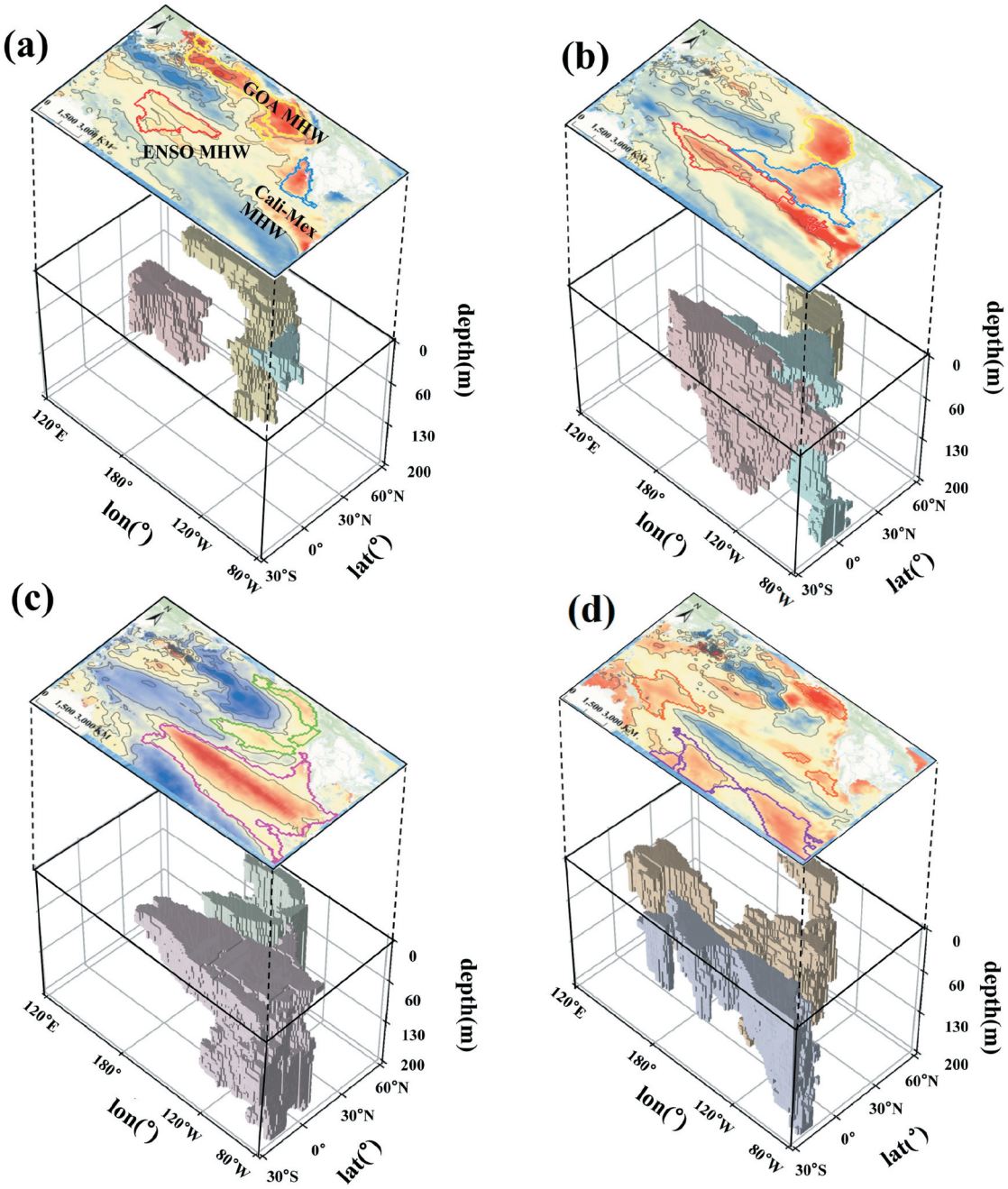

Figure 8. SSTA contours (0.5°C intervals) amd fine-grained MHWs at (a) June 2014, (b) April 2015, (c) February 2016 and (d) October 2016.

volume in September 2015. Referring again to Figure 9(a-b), the Cali-Mex MHW originated from a coastal MHW at 15°–30° latitude, rather than extending from the GOA MHW. In September 2015, Cali-Mex MHW exhibited two intensity centers between 0 m–70 m. As one of the nodes gradually decreased in size, its skeleton transformed from a Y-shape to I-shape. As depicted in Figure 10(d), the ENSO MHW formed through the merger of two sub-MHWs, one at the sea surface and another below 100 m. Compared to the other two MHWs, the skeleton of ENSO MHW displayed the steepest slope. Although the ENSO-related MHW exhibited significantly higher intensity than the other two events during its peak period, its intensity declined more rapidly after October 2016 (Figure 10(e)).

Both the temporal transitions and structural characteristics of MHW skeletons exhibit notable spatio-temporal variability. Regionally, events such as ENSO-related MHWs display frequent merging and splitting behaviors, reflecting complex interactions and broad spatial influence, while coastal MHWs (e.g. GOA) show greater temporal continuity with a predominance of continuation transitions. Temporally, merging events are more common during phases of intensification, whereas splitting transitions increase during decay periods. In terms of

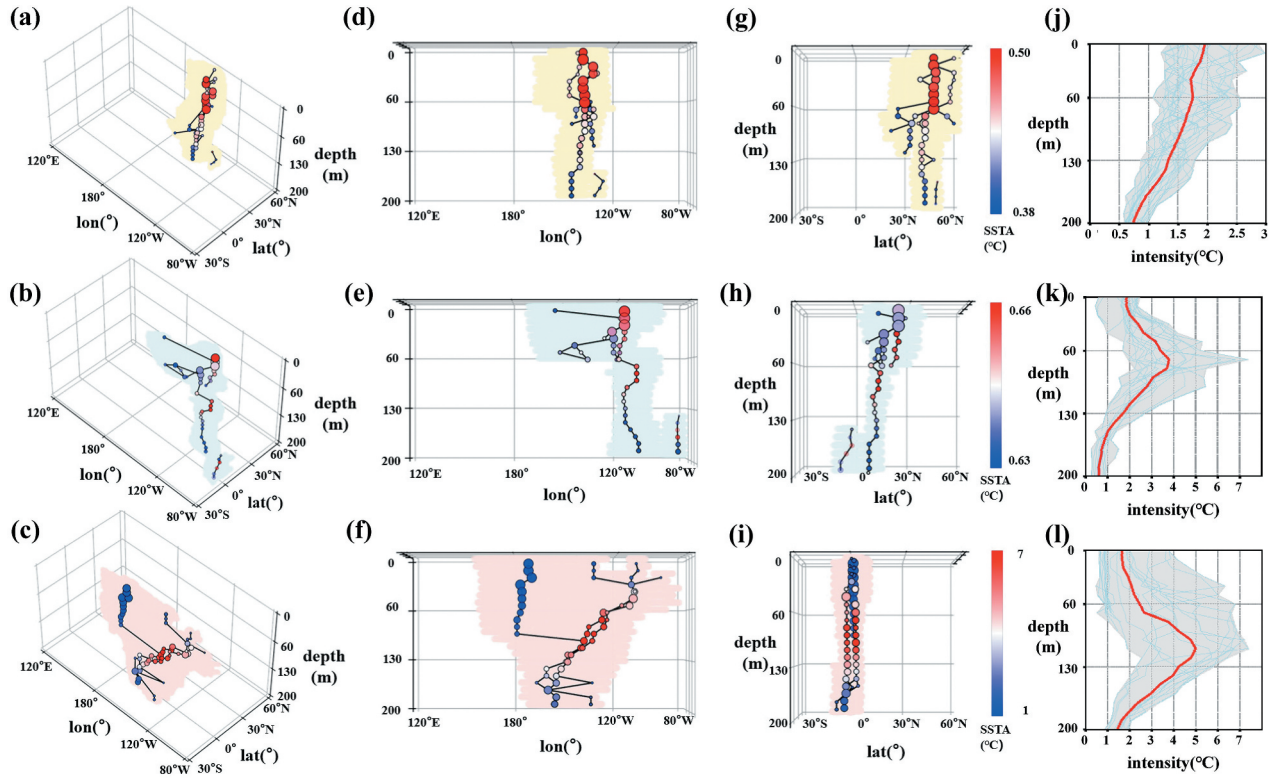

Figure 9. (a)–(c) three-dimensional, (d)–(f) longitude-depth profile, (g)–(i) latitude-depth profile and (j)–(l) vertical intensity profiles of the skeletons of the GOA MHW, cali-mex MHW and ENSO MHW at April 2015. The color of the node represents MHW intensity, and the size of the node represents MHW size.

structural evolution, the GOA MHW maintained a relatively stable vertical extent (~200 m) throughout its development, whereas the Cali-Mex and ENSO MHWs exhibited significant deepening over time. I-shaped skeletons tend to characterize stable, long-lived events, while Y-shaped skeletons are more typical of transitional phases involving structural reorganization.

3.4. Parameter sensitivity analysis

To ensure the robustness and reliability of the proposed 3D MHW skeleton construction method, we conducted a sensitivity analysis on key parameters involved in the preprocessing and segmentation stages. Specifically, we tested the sensitivity of (1) the neighborhood size used in KNN smoothing (Section 3.4.1) and (2) the moving window size for identifying local maximum intensity peaks as skeleton nodes (Section 3.4.2). These experiments aim to justify the chosen parameter settings and provide guidance for potential adaptation in future studies.

3.4.1. K-parameter of KNN smoothing

The KNN smoothing algorithm is designed to enhance the spatial coherence of the binary MHW field by suppressing isolated grid anomalies. We evaluated K values corresponding to $3 \times 3 \times 3$, $5 \times 5 \times 5$, and $9 \times 9 \times 9$ neighborhoods. As shown in Figure 11, a K value of $5 \times 5 \times 5$ was found to strike the optimal balance, which effectively filters out small, noisy features while preserving the spatial integrity of major MHW events. In contrast, the smaller window ($3 \times 3 \times 3$) allowed excessive noise, while the larger one ($9 \times 9 \times 9$) overly smoothed the field and distorted important substructures. The selected configuration ($5 \times 5 \times 5$) ensures the resulting MHW candidates remain physically interpretable and spatially consistent.

3.4.2. Moving-window size for intensity peaks extraction

To extract local thermal centers as skeleton nodes, we tested three moving window sizes: 2×5, 3×10, and 5×15 (latitude × longitude). As shown in Figure 12, a window of 3×10 provided the most satisfactory results. This setting minimizes over-fragmentation while still capturing the major intensity peaks within an MHW candidate. A smaller window (2×5) resulted in excessive seed points and fragmented skeletons, whereas a larger window (5×15) missed meaningful substructures by merging distinct centers. Our analysis indicates that the 3×10 configuration closely aligns with the spatial characteristics of STA contours. Importantly, the level of granularity in the skeleton representation is sensitive to this parameter,

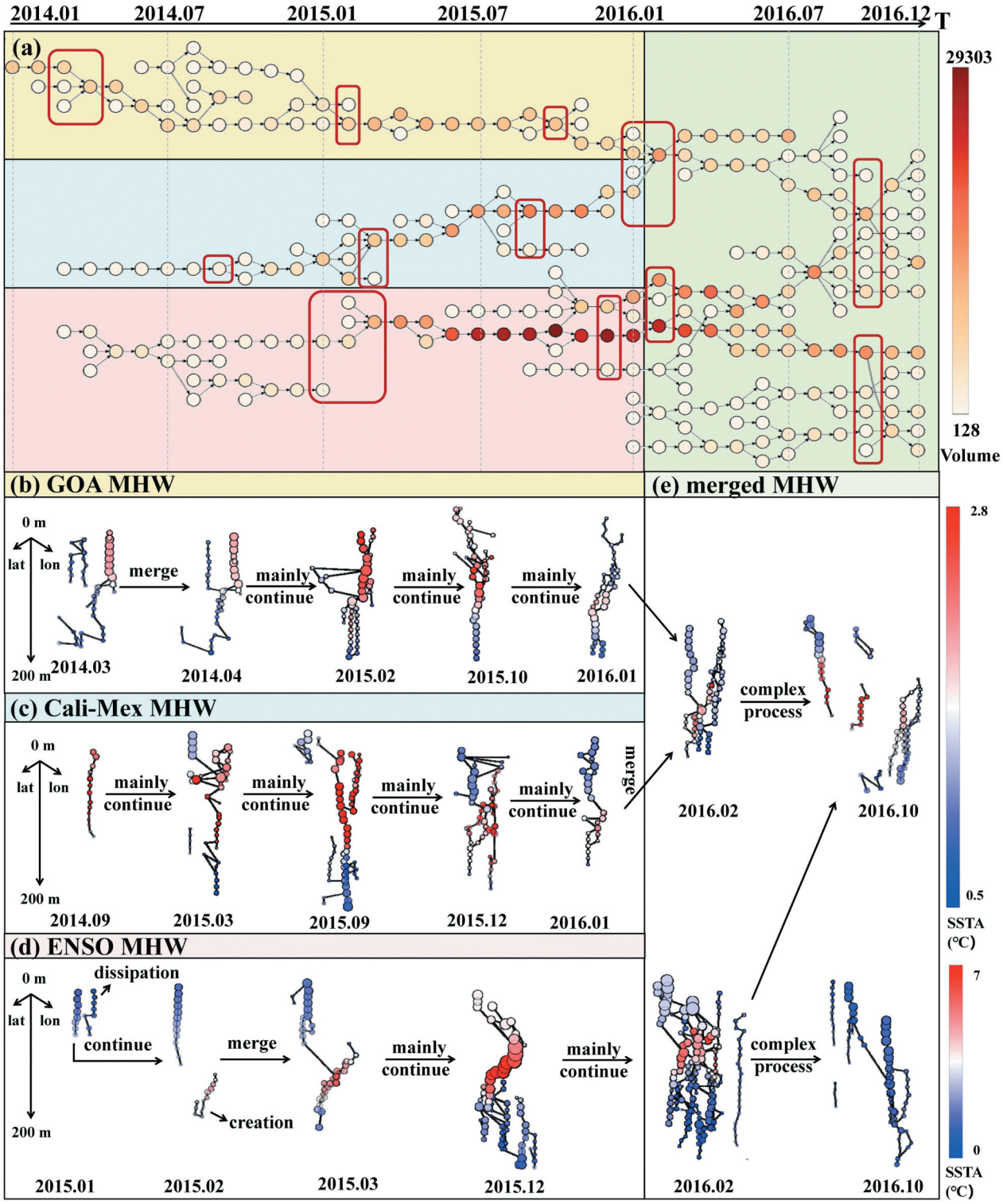

Figure 10. Evolution of MHW skeletons. (a) the evolution diagram, each node represents a 3D MHW snapshot at a certain time slice, and the color of the node represents the volume of the MHW. Skeletons of (b) GOA MHW, (c) Cali-Mex MHW, (d) ENSO MHW and (e) merged complex MHW.

suggesting potential for future work in scale-adaptive skeleton construction to analyze the multi-scale vertical structural characteristics of MHWs.

4. Discussion

The proposed skeleton method, characterized by its reconstructability and reliability, serves as an effective tool for capturing the internal structure of 3D MHWs. By simplifying the complex 3D MHW into a graph structure, the skeleton retains critical attributes such as intensity distribution, vertical stratification, and spatial extent. This method can be easily extended to other 3D geographical phenomena such as dust storms and their 4D evolution (Yue et al. 2017; Yu, Yang, and Jin 2018). Unlike traditional methods, such as centroids (Leborgne et al. 2018),

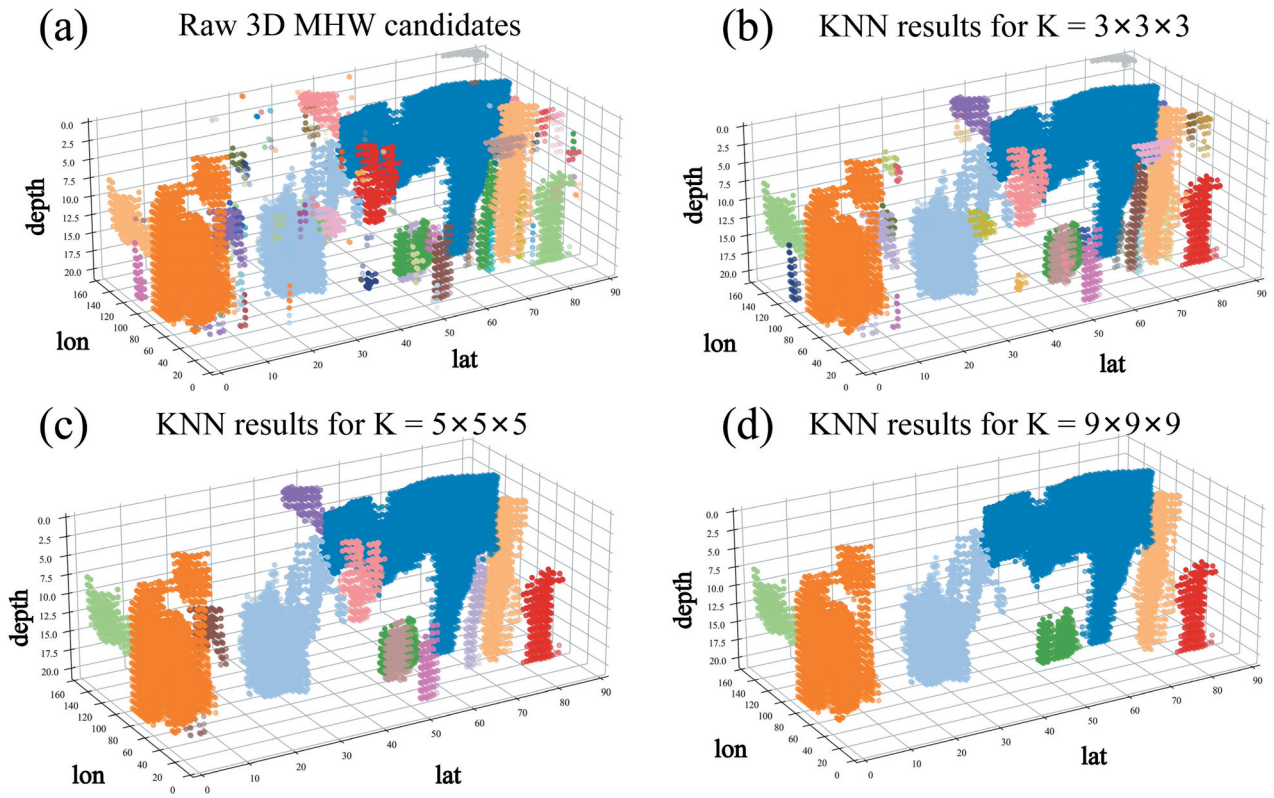

Figure 11. Sensitivity analysis results on the K-parameter in the KNN. (a) Raw MHW candidates on March, 2014 and (b-d) the post-processed snapshots by the KNN using different values for the K parameter.

that fail to represent 3D geographic events with significant heterogeneity and complex dimensional features, the skeleton offers a more robust and accurate alternative.

The skeleton-based analysis revealed key structural commonalities across the studied MHWs. All three MHWs exhibited foundational I-shaped and Y-shaped skeleton forms, reflecting their fundamental and multi-centered configurations. The branching structure of Y-shape is attributed to variations in heat distribution and ocean dynamics across depths, consistent with previous studies that highlight the influence of upper-ocean stratification and subsurface heat transport on MHW morphology (Capotondi et al. 2024). In addition to these commonalities, distinct individual evolutionary patterns and structure characteristics were observed among the MHWs. Cali-Mex MHW originated as a coastal MHW at 15°–30° latitude and evolved vertically from the surface to the ocean's interior. In contrast, the GOA MHW emerged from the merger of three smaller MHWs, while the ENSO-driven MHW formed through the combination of two sub-MHWs-one at the surface and another below 100 m. Notably, ENSO-driven MHW exhibited the steepest skeleton slope (up to 120 degrees) in the longitude-depth profile, reflecting a significant east-to-west shift of its intensity centers from surface to subsurface layers, which is consistent with the distribution of the shallow eastern and deep western thermocline in the tropical Pacific Ocean (An and Jin 2001). These findings support the physical plausibility of the identified skeleton structures and highlight the value of incorporating 3D structural analysis to better capture the complexity and variability of MHW development.

While the skeleton framework offers a novel approach to representing the internal 3D structure of MHWs from a data-driven perspective, several limitations remain. First, the current algorithm is statistical in nature and does not directly incorporate oceanographic processes such as stratification and vertical advection. Consequently, aggregating events using purely spatial-temporal criteria may conflate distinct phenomena driven by separate physical mechanisms. The current reliance on statistical metrics for skeleton edge construction, such as overlapping area ratios and geometric similarity, also simplifies vertical heat transport processes, omitting regional variations in vertical mixing, stratification, and lagged responses. Future enhancements should incorporate reanalysis-derived vertical velocities to enhance physical consistency. Second, the present analysis is constrained to specific oceanic regions and relied on available temperature datasets, which may not fully capture the coupled physical, biological, and chemical processes interacting with MHWs. Expanding the framework to incorporate additional datasets (e.g. ORAS5, GLORYS, SODA) and broader spatio-temporal domains would enhance its applicability to global ocean extremes. Third, the monthly resolution precludes precise duration estimates for short-lived MHWs. While our

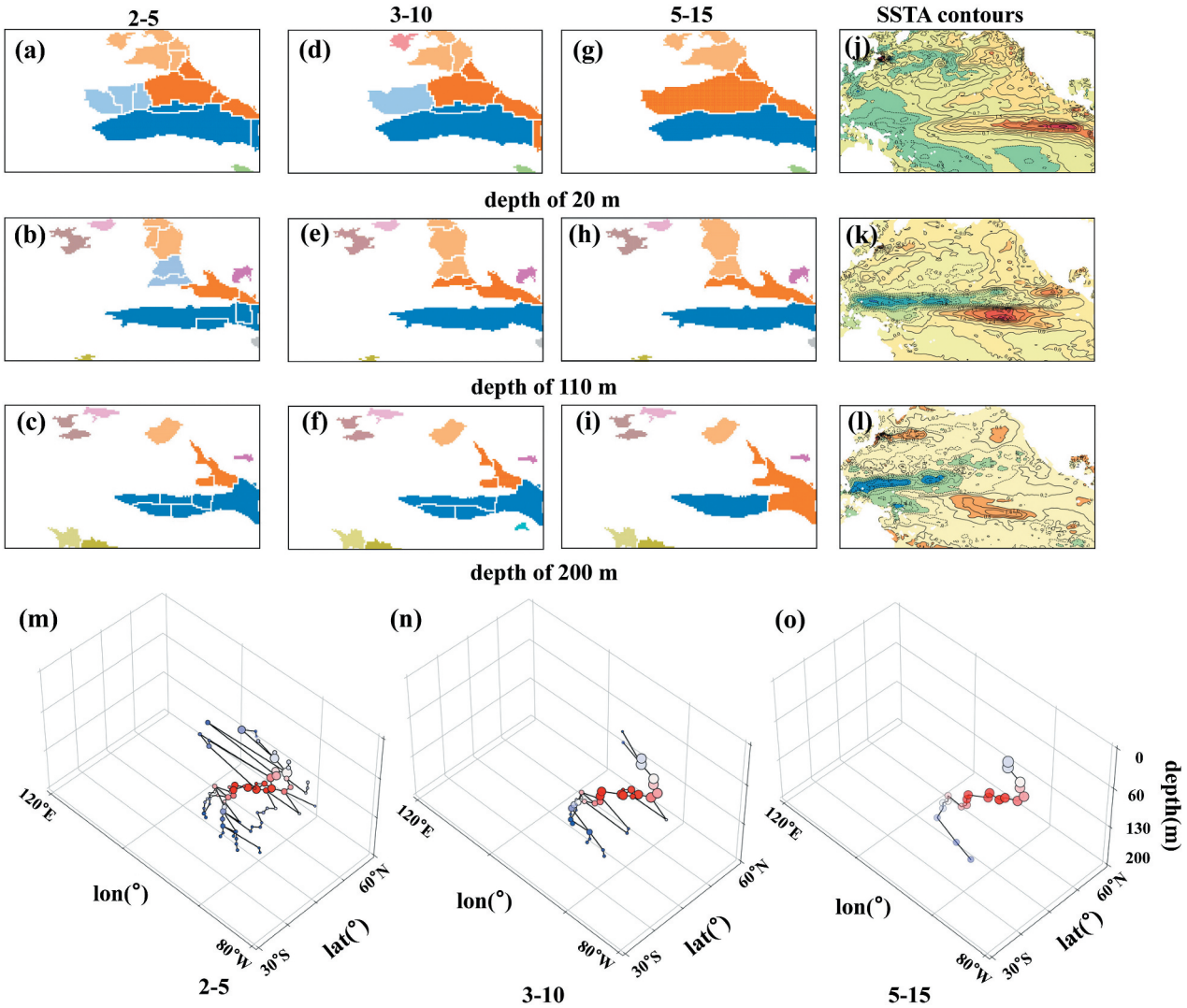

Figure 12. Sensitivity analysis results on the moving window size used for identifying local maximum intensity points at August 2015. MHW recognition results using a moving-window size of (a–c) 2 x 5, (d–f) 3 x 10 and (g–i) 5 x 15 at depth of 20 m, 110 m and 200 m; (j–l) SSTA contours at the same depths for comparison; (m–o) multi-scale MHW skeletons constructed across these configurations.

framework is adaptable to daily SST data, future implementation at higher temporal resolution is necessary to resolve short-term dynamics. Finally, the current framework focuses on structural extraction from discrete time slices without accounting for temporal continuity in clustering, which may limit its ability to capture the full evolution of MHWs. Future developments can extend the skeleton-based model by integrating temporal consistency using consensus graphs (Lancichinetti and Fortunato 2012). Such an extension would facilitate the identification of temporally stable, physically coherent MHW systems.

5. Conclusions

This study introduces a geospatial skeleton framework to represent and analyze the 3D structure and evolution of MHWs from a data-driven perspective. The proposed method transforms complex thermal anomalies into interpretable graph structures, enabling structured analysis of their spatial organization and temporal progression. Applied to three representative MHW events, the framework reveals distinct vertical architectures and highlights dynamic processes such as merging and splitting among subsurface MHWs.

Overall, this framework provides a novel and robust approach for resolving the 3D structure and dynamics of MHWs. Future developments may involve integrating the framework with physical ocean models and extending its application to broader spatio-temporal scales. Furthermore, enhancing the framework into a four-dimensional (4D) clustering approach that explicitly incorporates time as a dimension would enable continuous tracking of MHW evolution across both space and

time. Beyond MHWs, this method also offers a transferable modeling strategy for other environmental extremes and contributes to the development of advanced methods for analyzing multi-dimensional geophysical processes.

Disclosure statement

No potential conflict of interest was reported by the author(s).

Funding

This work was supported by the National Key Research and Development Program of China [grant number 2022YFB3904102].

Data and code availability statement

IAP temperature 1° gridded analysis product (IAPv4, http://www.ocean.iap.ac.cn/ftp/cheng/IAPv4_IAP_Temperature_gridded_1month_netcdf/.) (Cheng et al. 2024) is used in this study to identify MHW events. All Python source codes used in this study are openly accessible via Figshare: https://doi.org/10.6084/m9.figshare.29322473.

References

An, S., and F. Jin. 2001. "Collective Role of Thermocline and Zonal Advective Feedbacks in the ENSO Mode*." *Journal of Climate* 43. https://doi.org/10.1175/1520-0442(2001)014<3421:CROTAZ>2.0.CO;2.

Borgefors, G., I. Nyström, and G. S. Di Baja. 1999. "Computing Skeletons in Three Dimensions." *Pattern Recognition* 32 (7): 1225–1236. https://doi.org/10.1016/S0031-3203(98)00082-X.

Capotondi, A., R. R. Rodrigues, A. Sen Gupta, J. A. Benthuysen, C. Deser, T. L. Frölicher, N. S. Lovenduski, et al. 2024. "A Global Overview of Marine Heatwaves in a Changing Climate." *Communications Earth & Environment* 5 (1): 1–17. https://doi.org/10.1038/s43247-024-01806-9.

Cheng, L., J. Abraham, K. E. Trenberth, J. Fasullo, T. Boyer, R. Locarnini, B. Zhang, et al. 2021. "Upper Ocean Temperatures Hit Record High in 2020." *Advances in Atmospheric Sciences* 38 (4): 523–530. https://doi.org/10.1007/s00376-021-0447-x.

Cheng, L., Y. Pan, Z. Tan, H. Zheng, Y. Zhu, W. Wei, J. Du, et al. 2024. "IAPv4 Ocean Temperature and Ocean Heat Content Gridded Dataset." *Earth System Science Data* 16 (8): 3517–3546. https://doi.org/10.5194/essd-16-3517-2024.

Di Lorenzo, E., and N. Mantua. 2016. "Multi-Year Persistence of the 2014/15 North Pacific Marine Heatwave." *Nature Climate Change* 6 (11): 1042–1047. https://doi.org/10.1038/nclimate3082.

Ding, L., G. Xiao, A. Pano, M. Fumagalli, D. Chen and Y. Feng. 2024. "Integrating 3D City Data Through Knowledge Graphs." *Geo-Spatial Information Science*: 1–20. https://doi.org/10.1080/10095020.2024.2337360.

Elzahaby, Y., and A. Schaeffer. 2019. "Observational Insight into the Subsurface Anomalies of Marine Heatwaves." *Frontiers in Marine Science* 6:6. https://doi.org/10.3389/fmars.2019.00745.

He, Q., W. Zhan, M. Feng, Y. Gong, S. Cai, and H. Zhan. 2024. "Common Occurrences of Subsurface Heatwaves and Cold Spells in Ocean Eddies." *Nature* 634 (8036): 1111–1117. https://doi.org/10.1038/s41586-024-08051-2.

Hobday, A. J., L. V. Alexander, S. E. Perkins, D. A. Smale, S. C. Straub, E. C. J. Oliver, J. A. Benthuysen, et al. 2016. "A Hierarchical Approach to Defining Marine Heatwaves." *Progress in Oceanography* 141:227–238. https://doi.org/10.1016/j.pocean.2015.12.014.

Holbrook, N. J., A. Sen Gupta, E. C. J. Oliver, A. J. Hobday, J. A. Benthuysen, H. A. Scannell, D. A. Smale, and T. Wernberg. 2020. "Keeping Pace With Marine Heatwaves." *Nature Reviews Earth & Environment* 1 (9): 482–493. https://doi.org/10.1038/s43017-020-0068-4.

Lakshmanan, V., K. Hondl, and R. Rabin. 2009. "An Efficient, General-Purpose Technique for Identifying Storm Cells in Geospatial Images." *Journal of Atmospheric and Oceanic Technology* 26 (3): 523–537. https://doi.org/10.1175/2008JTECHA1153.1.

Lancichinetti, A., and S. Fortunato. 2012. "Consensus Clustering in Complex Networks." *Scientific Reports* 2 (1): 336. https://doi.org/10.1038/srep00336.

Leborgne, A., J. Mille, L. Tougne, J. Zhang, M. Xiong, C. Yin, and S. Gan. 2018. "Inner Shelf Response to Storm Track Variations Over the East Leizhou Peninsula, China." *International Journal of Applied Earth Observation and Geoinformation* 71:56–69. https://doi.org/10.1016/j.jag.2018.03.011.

Li, X., M. Feng, Y. Ran, Y. Su, F. Liu, C. Huang, H. Shen, et al. 2023. "Big Data in Earth System Science and Progress Towards a Digital Twin." *Nature Reviews Earth & Environment* 4 (5): 319–332. https://doi.org/10.1038/s43017-023-00409-w.

Meyer, F. 1992. "Color Image Segmentation." *1992 International Conference on Image Processing and its Applications*, (303–306). https://ieeexplore.ieee.org/document/785528/authors#authors.

Oliver, E. C. J., M. T. Burrows, M. G. Donat, A. Sen Gupta, L. V. Alexander & S. E. Perkins-Kirkpatrick. 2024. "Projected Marine Heatwaves in the 21st Century and the Potential for Ecological Impact." *Frontiers in Marine Science* 6:734. https://doi.org/10.3389/fmars.2019.00734.

Oliver, E. C. J., M. G. Donat, M. T. Burrows, P. J. Moore, D. A. Smale, L. V. Alexander, J. A. Benthuysen, et al. 2018. "Longer and More Frequent Marine Heatwaves Over the Past Century." *Nature Communications* 9 (1): 1324. https://doi.org/10.1038/s41467-018-03732-9.

Peizhi, H., and P.-C. Lai. 2002. "The Derivation of Skeleton Lines for Terrain Features." *Geo-Spatial Information Science* 5 (2): 68–73. https://doi.org/10.1007/BF02833889.

Que, X., F. Checconi, F. Petrini, and J. A. Gunnels. 2015. "Scalable Community Detection with the Louvain Algorithm." *2015 IEEE International Parallel and Distributed Processing Symposium*, 28–37. https://doi.org/10.1109/IPDPS.2015.59.

Reddy, P. J., S. E. Perkins-Kirkpatrick, and J. J. Sharples. 2022. "Interactive Influence of ENSO and IOD on Contiguous Heatwaves in Australia." *Environmental Research Letters* 17 (1): 014004. https://doi.org/10.1088/1748-9326/ac3e9a.

Ren, J., C. Wang, and Y. Yao. 2025. "Spatiotemporally Continuous Marine Heatwaves: A Novel Clustering Approach Reveals Increasing Frequency, Duration, Area, Intensity, and Movement Distance." *Geophysical*

Research Letters 52 (8): e2024GL113211. https://doi.org/10.1029/2024GL113211.

Scannell, H. A., G. C. Johnson, L. Thompson, J. M. Lyman, and S. C. Riser. 2020. "Subsurface Evolution and Persistence of Marine Heatwaves in the Northeast Pacific." *Geophysical Research Letters* 47 (23): e2020GL090548. https://doi.org/10.1029/2020GL090548.

Schaeffer, A., A. Sen Gupta, and M. Roughan. 2023. "Seasonal Stratification and Complex Local Dynamics Control the Sub-Surface Structure of Marine Heatwaves in Eastern Australian Coastal Waters." *Communications Earth & Environment* 4 (1): 1–12. https://doi.org/10.1038/s43247-023-00966-4.

Shu, H. 2016. "Big Data Analytics: Six Techniques." *Geo-Spatial Information Science* 19 (2): 119–128. https://doi.org/10.1080/10095020.2016.1182307.

Smith, K. E., M. T. Burrows, A. J. Hobday, N. G. King, P. J. Moore, A. Sen Gupta, M. S. Thomsen, T. Wernberg, and D. A. Smale. 2023. "Biological Impacts of Marine Heatwaves." *Annual Review of Marine Science* 15 (1): 119–145. https://doi.org/10.1146/annurev-marine-032122-121437.

Smith, K. E., M. T. Burrows, A. J. Hobday, A. Sen Gupta, P. J. Moore, M. Thomsen, T. Wernberg, and D. A. Smale. 2021. "Socioeconomic Impacts of Marine Heatwaves: Global Issues and Opportunities." *Science* 374 (6566). https://doi.org/10.1126/science.abj3593.

Sun, D., Z. Jing, F. Li, and L. Wu. 2023. "Characterizing Global Marine Heatwaves Under a Spatio-Temporal Framework." *Progress in Oceanography* 211:102947. https://doi.org/10.1016/j.pocean.2022.102947.

Sun, D., F. Li, Z. Jing, S. Hu, and B. Zhang. 2023. "Frequent Marine Heatwaves Hidden Below the Surface of the Global Ocean." *Nature Geoscience* 16 (12): 1099–1104. https://doi.org/10.1038/s41561-023-01325-w.

Tseng, Y.-H., R. Ding, and X. Huang. 2017. "The Warm Blob in the Northeast Pacific—The Bridge Leading to the 2015/16 El Niño." *Environmental Research Letters* 12 (5): 054019. https://doi.org/10.1088/1748-9326/aa67c3.

Xu, Q., K. Liu, H. Wang, and X. Chen. 2024. "Vertical Structures and Drivers of Marine Heatwaves and Cold-Spells in the Kuroshio Extension Region." *Environmental Research Letters* 19 (5): 054015. https://doi.org/10.1088/1748-9326/ad3b26.

Yu, M., C. Yang, and B. Jin. 2018. "A Framework for Natural Phenomena Movement Tracking – Using 4D Dust Simulation as an Example." *Computers & Geosciences* 121:53–66. https://doi.org/10.1016/j.cageo.2018.10.003.

Yue, H., C. He, Y. Zhao, Q. Ma, and Q. Zhang. 2017. "The Brightness Temperature Adjusted Dust Index: An Improved Approach to Detect Dust Storms Using MODIS Imagery." *International Journal of Applied Earth Observation and Geoinformation* 57:166–176. https://doi.org/10.1016/j.jag.2016.12.016.

Zhang, C., D. Wang, Z. Liu, S. Lu, C. Sun, Y. Wei, and M. Zhang. 2020. "Global Gridded Argo Dataset Based on Gradient-Dependent Optimal Interpolation." *Journal of Marine Science and Engineering* 10 (5): 650. https://doi.org/10.3390/jmse10050650.

Zhang, Y., Q. Zhu, G. Liu, W. Zheng, Z. Li, and Z. Du. 2011. "Geoscope: Full 3D Geospatial Information System Case Study." *Geo-Spatial Information Science* 14 (2): 150–156. https://doi.org/10.1007/s11806-011-0478-z.

Zhang, Y., Y. Du, M. Feng, and A. J. Hobday. 2023. "Vertical Structures of Marine Heatwaves." *Nature Communications* 14 (1): 6483. https://doi.org/10.1038/s41467-023-42219-0.

Zou, X., X. Liu, M. Liu, L. Tian, L. Zhu, and Q. Zhang. 2023. "Spatiotemporal Graph-Based Analysis of Land Cover Evolution Using Remote Sensing Time Series Data." *International Journal of Geographical Information Science* 37 (5): 1009–1040. https://doi.org/10.1080/13658816.2023.2168006.

Žunić, J., K. Hirota, and P. L. Rosin. 2010. "A Hu Moment Invariant as a Shape Circularity Measure." *Pattern Recognition* 43 (1): 47–57. https://doi.org/10.1016/j.patcog.2009.06.017.